Low-Cost PCB Integrated Inductive Sensor for Radial Rotor Displacement Measurement

Dominik WIMMER, Markus HUTTERER, Manfred SCHRÖDL
TU Wien, Institute of Energy Systems and Electrical Drives,
Gußhausstraße 25-29, 1040 Vienna, Austria, dominik.wimmer@tuwien.ac.at

Abstract

Active magnetic bearings require position feedback to enable a stable control of a levitating rotor. The position information can be provided by explicit position sensors or the usage of self-sensing techniques. This study deals with a PCB integrated inductive sensor design for radial rotor displacement measurement. The sensor design consists of a six-pole stator arrangement, a soft magnetic rotor ring as measurement target as well as a PCB integrated coil configuration. The sensor principle is based on the detection of inductance deviations of an eccentrical levitating rotor. The surrounding stator poles of the sensor enable a large and distributed measurement area which allows a suppression of imperfections on the rotor surface. Concerning design optimization, a short axial sensor length is aspired to enable a less construction space consuming sensor integration compared to conventional inductive sensor designs. Thus, a smaller sensor enables the possibility of shorter rotor shaft designs to overcome challenges of flexible rotor characteristics or inadmissible axial thermal expansion. This study covers an introduction to the sensor's working principle, design considerations as well as an experimental verification of a PCB integrated inductive sensor prototype.

1. Introduction

Active magnetic bearings (AMBs) are a well-suited technology for contact-free suspension of rotors with high rotational speeds. Due to the open loop instability of AMBs, the rotor position must be fed back to a controller to enable a stable operation. Conventional position sensors for AMBs often rely on an electromagnetic sensor principle, whereby eddy current sensors [1-5] and inductive sensors [6-9] are widely spread in research and industrial applications. Besides conventional position sensors, also self-sensing methods have been evolved for rotor position detection [10]. Position sensors in AMB applications usually have to fulfill high demands concerning sensor linearity, sensor noise, measurement bandwidth, low-cost design, EMI immunity as well as a small construction space. Considering a typical AMB application, the length of the shaft is determined by the size of the drive, radial bearings, thrust bearings, auxiliary bearings, position sensors and e.g. turbine blades. In this regard, long rotor shafts can cause problems concerning axial thermal expansion and flexible modes of the rotor. Therefore, it is desired that the position sensors can be integrated within a small axial construction space.

This study deals with a low-cost PCB integrated sensor design for radial rotor displacement measurement. Although this work is about the design of an inductive sensor, the sensor principle is strongly related to self-sensing position detection of radial AMBs. In previous work, the self-sensing control of a homopolar radial AMB was conducted by the measurement of inductance deviations of an eccentrically levitating rotor [11]. Therefore, the position-dependent inductance deviations were determined by differential current slope measurements of opposing bearing coils. Since the self-sensing control showed appropriate results in previous investigations, the sensor principle of this study is based on differential current slope measurements. Concerning the sensor design, the focus was set to low-cost design and minimal axial construction space. Furthermore, the sensor design features an integral measurement over several poles which enables a suppression of imperfections of the rotor surface. In the following, the sensor operation principle, design considerations as well as measurement results are outlined.

2. Sensor Design and Principle of Operation

Figure 1 shows an illustration of a six-pole PCB integrated sensor design for position measurement of a rotor shaft. The sensor consists of a flexible print circuit board with a ferromagnetic core inlay. Therefore, the coils of the flexible PCB are folded around the poles of the ferromagnetic core. The usage of a multilayer PCB design enables a high number of coil turns even in applications with highly restricted construction space. The sensor

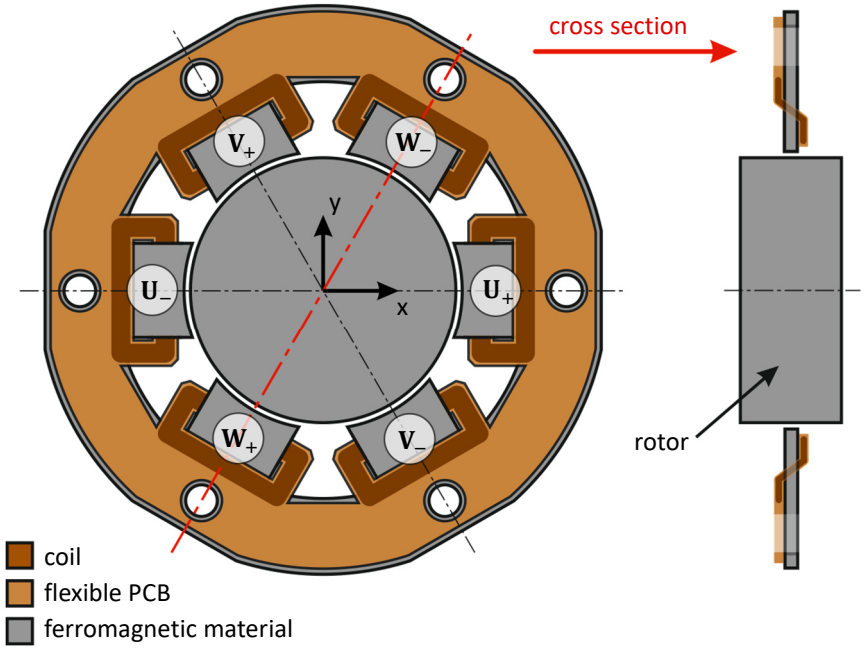

Fig. 1: Six-pole radial inductive sensor design with flexible PCB integrated coils.

principle relies on the measurement of inductance deviations of the sensor coils caused by an eccentrically levitating rotor. In this configuration, the sensor coils are wired in a double wye configuration ($\mathbf{U}_+, \mathbf{V}_+, \mathbf{W}_+$ and $\mathbf{U}_-, \mathbf{V}_-, \mathbf{W}_-$). Figure 2 shows the topology of the sensor circuit. The sensor coils are excited by a three-phase rectangular voltage pulse pattern and the rotor position is obtained by the use of differential current slope

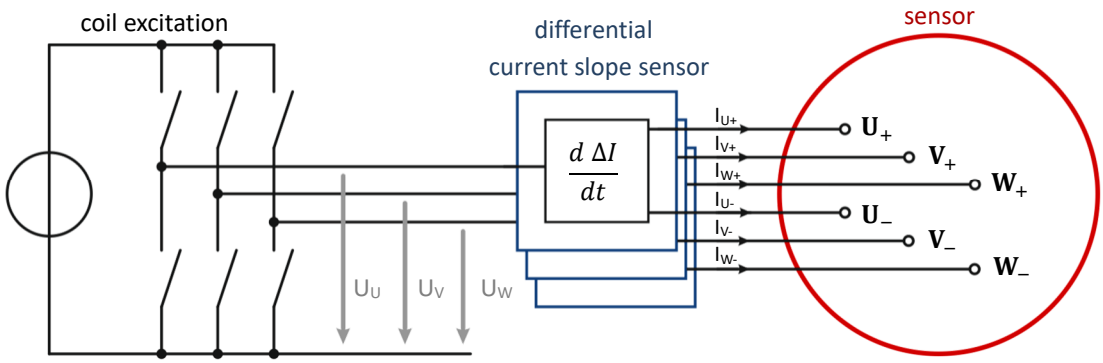

Fig. 2: Topology of the sensor circuit with rectangular coil voltage excitation and current slope measurement.

sensors [12]. Figure 3 shows an illustration of the coil voltages and the corresponding currents of the phase U in case of an eccentrically levitating rotor. It can be seen that the currents of opposing coils exhibit a different current slope. According to [9], the actual rotor position can be derived by the current slope signals. In approximation, the relationship between the position dependent inductance $L(x, y)$ and the differential current slope $\Delta I(t)$ is given by equation (1).

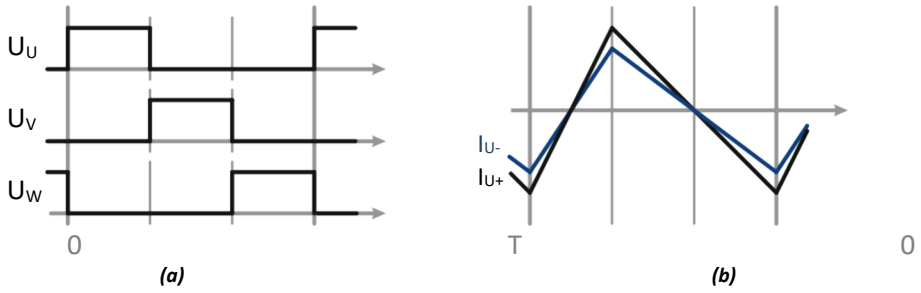

Fig. 3: ***(a)*** *Sensor coil voltage excitation* ***(b)*** *Current profile in opposing coils in case of an eccentrical rotor position*

$$L(x,y) \approx U(t)\left(\frac{d\,\Delta I(t)}{dt}\right)^{-1}, \quad \Delta I = I_+ - I_- \tag{1}$$

For more detailed considerations concerning position calculation the complete reluctance network of the sensor arrangement must be taken into account, which is not outlined for reasons of complexity. Table 1 shows the sensor specification for a stator core thickness of 1.6 mm, which was the thinnest core in this investigation. The measurement results will also show a comparison with a core with 4 mm thickness.

Table 1: Sensor specification

Symbol	***Parameter***	***Value***
z	Axial sensor length	1.9 mm
z_S	Sensor core thickness	1.6 mm
z_{PCB}	Flex-PCB thickness	0.15 mm
d_O	Outer sensor diameter	90 mm
d_I	Inner sensor diameter	44 mm
d_R	Rotor diameter	42.6 mm
$\Delta x, \Delta y$	Rotor displacement	+/- 700 µm
N	Turns per pole	46
f_{coil}	Coil switching frequency	40 kHz

3. Sensor Prototype

The main element of the prototype is a flexible PCB which contains the sensing coils, the coil connections as well as the sensor cable. The PCB is manufactured as a single element and the flexible design enables an easy assembly by simply bending the coil edges over a ferromagnetic core as shown in Fig. 4(a). Figure 4(b) shows the sensor electronics which contains differential current slope sensors and a microcontroller for signal processing.

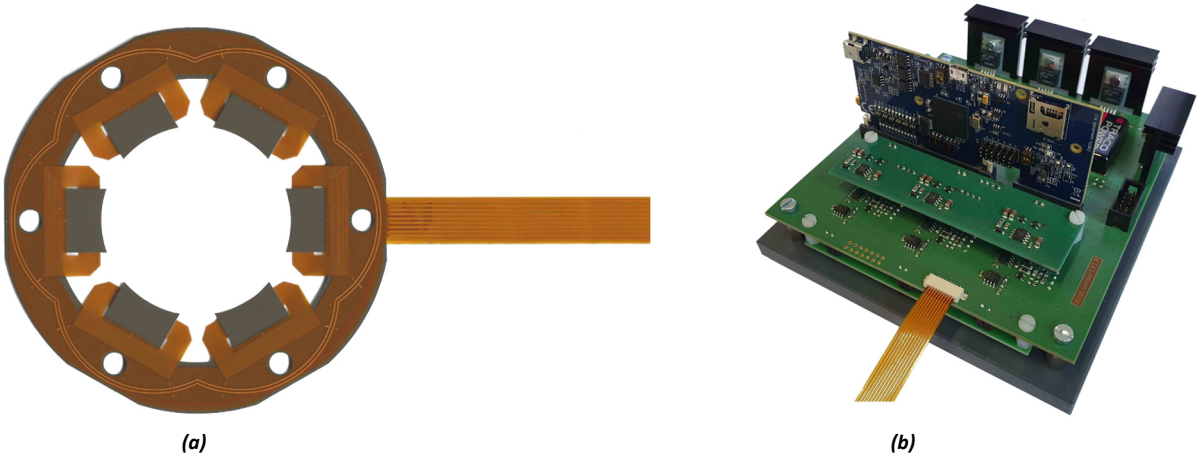

Fig. 4: ***(a)*** *Sensor prototype with flexible PCB integrated coils* ***(b)*** *Sensor electronics*

In this study, different ferromagnetic stator cores were investigated regarding their suitability for sensor operation. Figure 5 shows three different stators, whereby the ferrite material was chosen to obtain a prototype with minimal eddy current effects for a feasibility study. In contrast, the laminated iron stators were chosen as candidates for a practical sensor application by reason of higher structural strength and low-cost manufacturing in larger quantities.

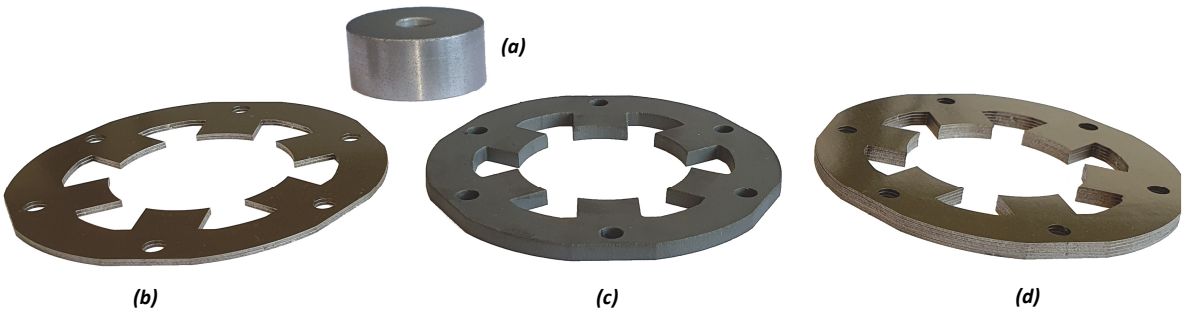

*Fig. 5: Flux guiding sensor elements: **(a)** soft magnetic composite rotor **(b)** laminated iron sheet stator with 1.6 mm thickness **(c)** ferrite stator with 4 mm thickness **(d)** laminated iron sheet stator with 4 mm thickness*

4. Measurements

In the first step, the different stator cores were analyzed concerning their frequency-dependent impedance characteristics. Figure 6 shows the impedance of a single sensing coil in case of centered rotor position. It can be seen that the ferrite core features the highest inductance and very little impact of eddy currents due to a maximum phase shift of nearly +90°. In contrast to the ferrite core, the laminated iron core with the same thickness of 4 mm exhibits a smaller impedance magnitude and a maximum phase shift of about 58°. As expected, the laminated iron core with 1.6 mm thickness has a lower inductance by less ferromagnetic material for flux

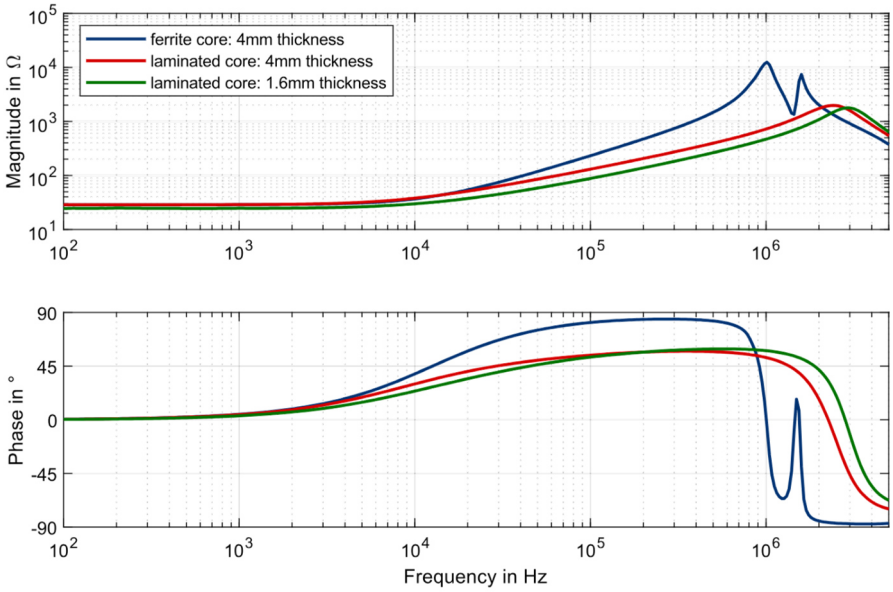

Fig. 6: Impedance characteristics of a single coil for different sensor core configurations (rotor at center position)

guidance. The 1.6 mm stator core also exhibits a slightly lower DC resistance due to a shorter coil winding length compared to the 4 mm stator. Furthermore, it can be seen for all stator configurations that the first resonance frequency is $\geq$1 MHz which provides a high separation margin for a sensor operating frequency of 40 kHz. For this reason, all three stator cores seem to be potential candidates for the sensor design.

In the next step, it was investigated if the measured transient sensor waveforms are consistent with an electrical

simulation model of the sensor, which also includes the entire reluctance network of the sensor coils. For this analysis, the ferrite stator was used to suppress eddy current effects which are very complex to be adequately described in an analytical way. Figure 7 shows the transient sensor characteristics for an eccentrically mounted rotor in respect to the electrical quantities of Fig. 2. For the comparison between the simulation results and the actual prototype behavior the measurement results of phase U are depicted. The upper plot of Fig. 7 shows the

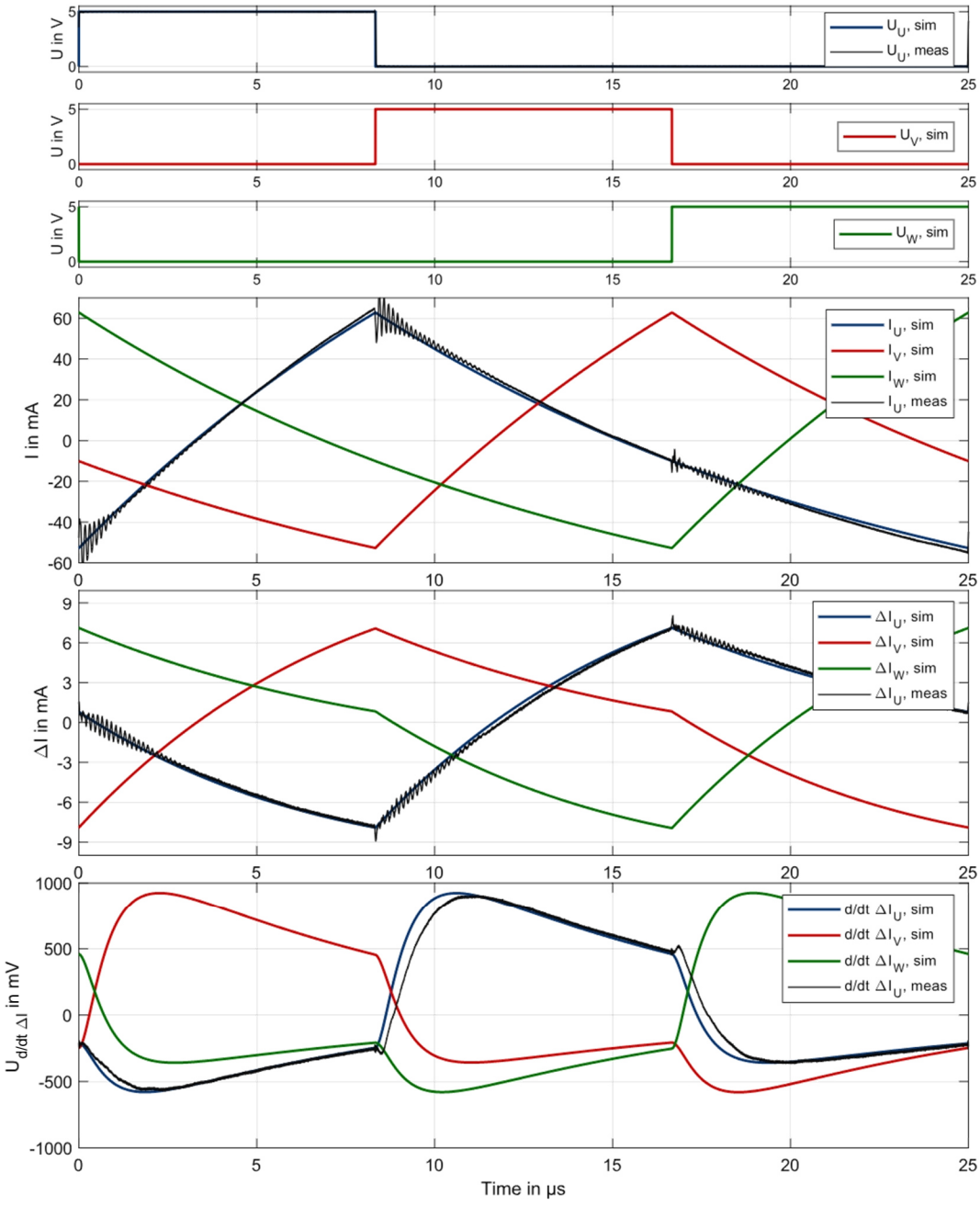

Fig. 7: Comparison of simulated and measured sensor signals for an eccentrical rotor position (4 mm ferrite stator)

staggered voltage pulses of the phases (U_U, U_V, U_W) which are generated by a low power inverter. In the following, it is distinguished between the phase currents (I_U, I_V, I_W) and the differential phase currents (ΔI_U, ΔI_V, ΔI_W). The phase currents are calculated by the sum of opposing coil currents e.g. $I_U = I_{U+} + I_{U-}$ and in contrast, the differential phase currents are calculated by a subtraction of opposing coil currents e.g. $\Delta I_U = I_{U+} - I_{U-}$. As it can be seen in Fig. 7, the differential currents are much smaller than the phase currents and result from an eccentrical rotor position. A differential current slope sensor [12] is used to obtain an output voltage which is proportional to the

differential current slope d/dt ΔI. The bottom plot of Fig. 7 shows the output voltage of the differential current slope sensor $U_{d/dt\ \Delta I}$ after signal conditioning which is used for position calculation in the microcontroller. It can be seen that there is a good match between simulation and measurement data for a given rotor eccentricity. Remaining deviations between simulation results and the measurements can be attributed to unconsidered stray flux paths, frequency depended material parameters, a simplified simulation model of the current slope sensor as well as a deviation between the simulated and the actual rotor position.

After the validation of the simulation model, a performance benchmark of the sensor prototype was carried out. Therefore, a linearity measurement for a linear and a circular movement as well as a noise analysis was conducted. For all measurements, the rotor was initially aligned to the stator center position within the mechanical tolerances of the test rig. The remaining alignment error was compensated for afterwards in the measurement data by an offset correction. Figure 8 shows the linearity analysis for a single axis movement for a sensor with laminated stator cores with different thicknesses (4 mm, 1.6 mm). It can be seen that both variants exhibit good

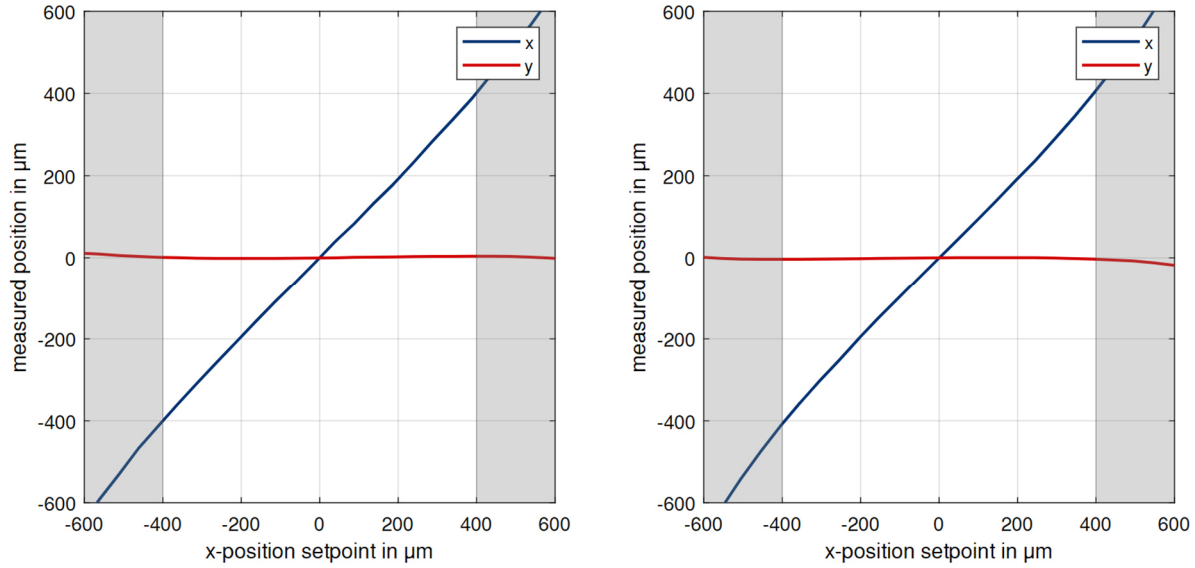

(a) ***(b)***

Fig. 8: Linearity analysis for single axis movement: ***(a)*** *4 mm laminated stator* ***(b)*** *1.6 mm laminated stator*

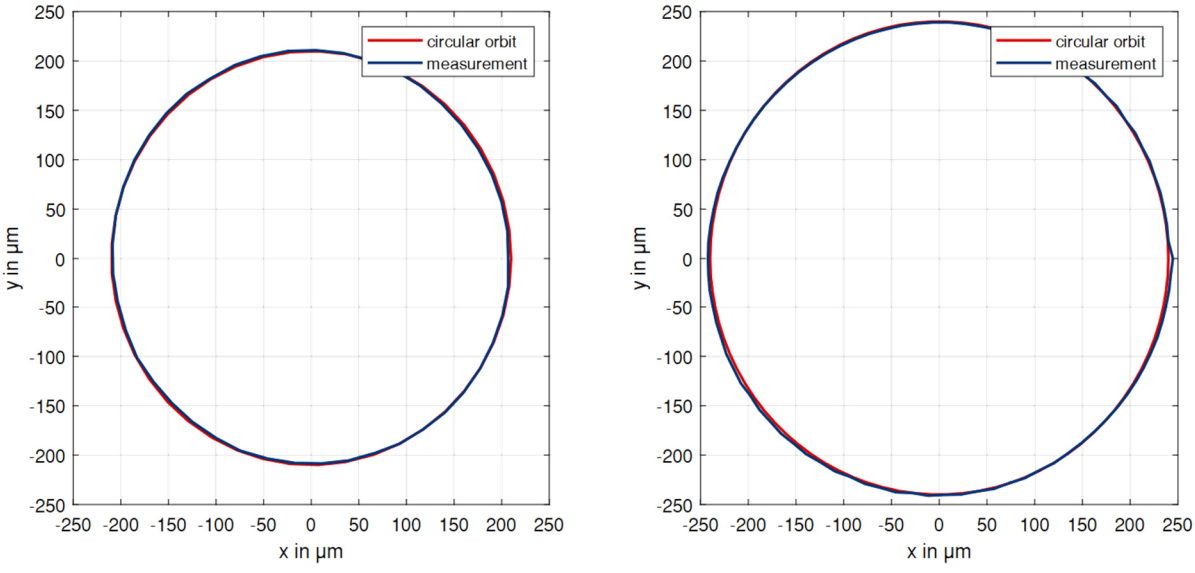

(a) ***(b)***

Fig. 9: Linearity analysis for circular trajectory: ***(a)*** *4 mm laminated stator (420 µm orbit)* ***(b)*** *1.6 mm laminated stator (480 µm orbit)*

linearity and little couplings to the perpendicular axis. The linearity error for a nominal movement of +/- 400 µm is smaller than 9 µm for both variants. In the following, the rotor was moved along a circular trajectory. Figure 9 shows the measured orbits (420 µm for 4 mm stator thickness, 480 µm for 1.6 mm stator thickness) in comparison to an ideal circle. Both sensor variants exhibit deviations from the ideal circle smaller than 5 µm.

Finally, a noise analysis of the position signal was performed. For this reason, the rotor was mounted at center position and the 100 000 measurement samples were recorded. Figure 10 shows the sample count distribution

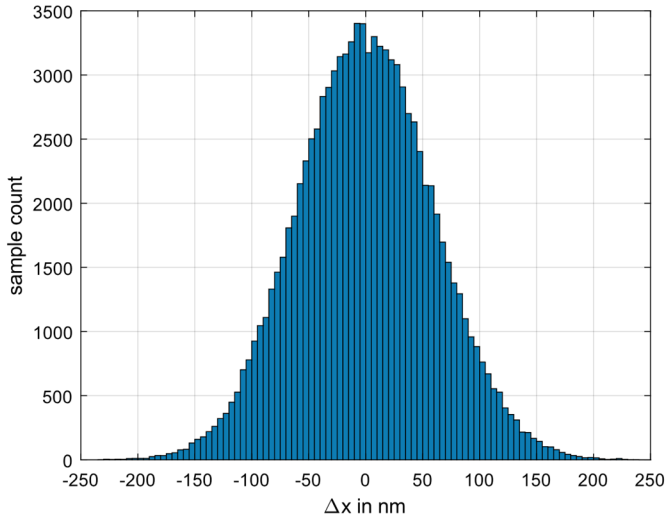

Fig. 10: Sample count distribution for noise analyses of 100 000 measurement samples (4 mm laminated stator, rotor at center position, 10 kHz measurement bandwidth)

for the laminated prototype with 4 mm stator core thickness. The noise distribution of the prototype with 1.6 mm stator thickness is not shown in detail, because the analog gain of the sensor electronics was optimized for the 4 mm prototype variant instead. However, it can be stated that the measurement showed 60 nm_{rms} sensor noise for the 4 mm prototype and 79 nm_{rms} sensor noise for the 1.6 mm prototype with a non-optimized analog circuit.

5. Conclusion

This study covers the design and experimental verification of a low-cost inductive sensor design for radial rotor displacement measurement. In contrast to conventional inductive sensor designs with wounded wire coils, the coils are integrated in a flexible PCB design. The flexible PCB design allows a well-defined geometry of the sensing coils as well as the possibility of an integration of the coil connections and the sensor cable as demonstrated on the prototype. The usage of a flexible PCB enables a sensor design with a very low axial dimension which can be beneficial for applications with limited construction space or the need of a reduction of the rotor length to overcome challenges in rotor dynamics.

The sensor design was experimentally investigated with different stator core configurations concerning their suitability for sensor operation. Measurements on a sensor prototype with a stator core thickness of 1.6 mm showed a low linearity error of 9 µm and a very low measurement noise of only 79 nm_{rms}. However, for a proper choice of the sensor stator core thickness, the effective measurement area on rotor material as well as the stray flux to pole flux ratio must be considered for practical applications. Finally, it can be stated that this sensor design seems to be a suitable candidate for radial displacement measurement in AMB applications. Future investigations will cover the influence of conductive or ferromagnetic parts in close proximity to the sensor coils. Furthermore, an analysis of potential temperature drifts and compensation techniques is aspired.

References

[1] Štusák, M. (2014), “Eddy current sensors for magnetic bearings of the textile spinning machines”, ISMB14, 14th International Symposium on Magnetic Bearings, Linz, Austria, August 11-14.

[2] Larsonneur, R. and Bühler, P. (2004), “New radial sensor for active magnetic bearings”, ISMB9, 9th International Symposium on Magnetic Bearings, Lexington, Kentucky, August 3-6.

[3] Wang, K., Zhang, L., Zheng, S., Zhou, J. and Liu, X. (2018), “Analysis and experiment of self-differential eddy current sensor for high-speed magnetic suspension electric machine”, IEEE Transactions on Industry Applications 55(3)

[4] Grobler, A. J., van Schoor, G. and Ranft, E. O. (2017), “Design and optimisation of a pcb eddy current displacement sensor”, SAIEE Africa Research Journal 108(1).

[5] Wimmer D., Hutterer M. and Schrödl M. (2023), “Design of a PCB integrated eddy current sensor with shield feature for radial rotor displacement measurement”, ISMB18, 18th International Symposium on Magnetic Bearings, Lyon, France, July 18-21.

[6] Mitterhofer H., Rakov M. and Gruber W. (2018), “Sum-flux rotor position sensor with self-balancing magnetic bearing concept”, ISMB16, 16th International Symposium on Magnetic Bearings, Beijing, China, August 13-17.

[7] Wang K., Zhang L., Le Y., Zheng S., Han B. and Jiang Y. (2017), “Optimized Differential Self-Inductance Displacement Sensor for Magnetic Bearings: Design, Analysis and Experiment”, IEEE Sensors Journal, vol. 17, no. 14

[8] Chen S. C., Le D. K. and Nguyen V. S. (2014), “Inductive Displacement Sensors with a Notch Filter for an Active Magnetic Bearing System”, MDPI, Sensors 2014, vol. 14, no. 7

[9] Fericean S. and Droxler R. (2007), “New Noncontacting Inductive Analog Proximity and Inductive Linear Displacement Sensors for Industrial Automation”, IEEE Sensors Journal, vol. 7, no. 11

[10] Maslen E. H. (2006), “Self–sensing for active magnetic bearings: overview and status”, ISMB10, 10th International Symposium on Magnetic Bearings, Martigny, Switzerland, August 21-23.

[11] Wimmer D., Hutterer M. and Schrödl M. (2021), “Space Vector Modulation for High Dynamic Current Control of a Self-Sensing Active Magnetic Bearing”, ISMB17, 17th International Symposium on Magnetic Bearings, Rio de Janeiro (online), Brazil, August 18-21.

[12] Wimmer D., Hutterer M. and Schrödl M. (2021), “Design and Analysis of a PCB Integrated Differential Current Slope Sensor with Ferrite Support for High dV/dt Operations”, PCIM Europe digital days 2021, May 3-7.